Int. J. Heat Mass Transfer. Vol. 33, No. 10, pp. 2275–2284, 1990
Printed in Great Britain

0017–9310/90 $3.00 + 0.00

Heat exchange between unequal countercurrent vessels asymmetrically embedded in a cylinder with surface convection

M. ZHU, S. WEINBAUM and L. M. JIJI
Department of Mechanical Engineering, The City College of the City University of New York, New York, NY 10031, U.S.A.

(*Received* 16 *May* 1989 *and in final form* 19 *December* 1989)

Abstract—A three-dimensional approximate analytic solution is presented for the unequal countercurrent heat transfer between parallel paired vessels asymmetrically embedded in a long cylinder with surface convection. The analysis assumes that the velocity profile in the vessels is parabolic, the Peclet number is large compared to unity and the radius of the cylinder is several times larger than the distances from the center of the cylinder to the vessels. A perturbation method is employed by taking the reciprocal of the Peclet number as a small parameter. The new solution approach takes into consideration the axial thermal interaction and describes the three-dimensional asymmetric thermal field due to the vessels, the wall temperatures of which are nonuniform in the cross-sectional plane. Application of the model to whole limb heat transfer is discussed.

1. INTRODUCTION

COUNTERCURRENT heat transfer has wide applications in industrial problems involving power plant steam and water distribution lines, insulation of electrical powerlines and certain types of heat exchangers. These more traditional applications are summarized in ref. [1]. A new area of application which has been the subject of numerous studies in the past decade is the countercurrent heat exchange between the larger countercurrent vessels of the microcirculation [2–11] as well as the major axial arteries and veins that supply the human limbs [12, 13]. The countercurrent heat exchange between the thermally significant vessels of the microcirculation has led to the development of a new bioheat equation to describe microvascular blood-tissue heat transfer and a fundamental expression for the effective conductivity of a medium in which there are small paired countercurrent vessels, the thermal relaxation lengths of which are small compared to the length scale of the medium [5].

Despite the extensive literature cited above there is no existing three-dimensional solution which considers the axial thermal interaction between the fluid in the countercurrent vessels when they are embedded in a cylinder of finite radius with a general convective boundary condition at the cylinder surface. This geometry can be considered as a basic prototype for the axial heat transfer in a human limb. Most previous studies of countercurrent heat exchange are either based on the two-dimensional conduction shape factors for embedded vessels and pipes in the cross-sectional plane or are simplified analyses of the axial interaction in which there is a linear axial temperature distribution. In refs. [6, 14, 15] approximate solutions are obtained for the conduction shape factors by superposing solutions for an infinite line source and sink in an infinite medium. Exact solutions for these shape factors in an infinite medium, based on the bicircular coordinate geometry, are presented in refs. [2, 4, 16, 17] for vessels with either constant wall temperature or constant heat flux. A related bicircular solution for a single buried pipe in a half space is given in Bau and Sadhal [18]. The latter solution is novel in that the temperature of the fluid in the pipe is matched with the surroundings and the wall temperature is nonuniform. In ref. [6] the axial interaction equations are formulated for an artery–vein pair and shape factors are derived for two equal sized vessels embedded in a surrounding tissue cylinder with constant wall temperature in the cross-sectional plane. The formulation for the axial interaction is based on a superposition which is a summation of the heat exchange between a perfect countercurrent heat exchanger and the heat loss from the vessel pair to the surface of the surrounding tissue cylinder. This analysis is extended in ref. [10] to vessels of unequal size which are at constant wall temperature and the theory used to formally derive an expression which relates the local artery–vein temperature difference to the axial gradient of the surrounding tissue temperature in the new Weinbaum–Jiji bioheat equation [5].

The motivation for the present study stems primarily from the new model for whole limb heat transfer proposed in ref. [13]. In this paper the Weinbaum–Jiji bioheat equation is applied outside a cylindrical core region which contains the large axial vessels of the limb. An important restriction on the core energy balance in this model is that it requires that the heat loss from these central vessels to the surrounding tissue be small compared to the heat exchange between the vessels. The numerical results in ref. [13] show that this assumption will not be satisfied when convective heat loss at the skin surface is important and that a

NOMENCLATURE

a	vessel radius (a and v)
A_{ij}	component of eigenvector, defined by equations (20) and (21)
Bi	Biot number of embedding medium cylinder
c_f	specific heat of fluid in vessels
C_i	constant, defined by equations (20) and (21)
h	heat transfer coefficient
k	thermal conductivity
k'	ratio of fluid and embedding medium thermal conductivities
Nu	Nusselt number of vessel
Pe	Peclet number of vessel a
q	rate of energy loss at vessel wall per unit length
Q_a	variable, defined by equation (12)
Q_v	variable, defined by equation (13)
r	radial coordinate
R	radius of embedding cylinder
s	distance between vessels
s_a	distance from origin to vessel a
s_v	distance from origin to vessel v
T	temperature
T_∞	environmental temperature
T_0	bulk temperature of vessel a at $Z = 0$
V	mean fluid flow velocity
V'	ratio of V_a to V_v
z	dimensionless axial coordinate
Z	axial coordinate.

Greek symbols

β	reciprocal of Peclet number
θ	dimensionless temperature
θ_p	variable, defined by equation (11)
λ_i	eigenvalue, defined by equation (22)
ρ	dimensionless radial coordinate
ρ_f	density of fluid in vessels
ρ_R	dimensionless radius of embedding cylinder
σ_c	shape factor between vessels
σ_t	shape factor between vessel pair and environment
ϕ	polar angle in cylindrical coordinates.

Superscript

$\bar{}$	dimensionless.

Subscripts

a	vessel a
b	bulk
f	fluid in vessels
m	mean value
t	embedding medium
v	vessel v
w	vessel wall
0	zeroth order.

more general theory is required for countercurrent heat exchange in a cylinder in which there is no restriction on the convective boundary condition at the cylinder surface. The solution in ref. [13] also assumes that the vessel wall temperatures are uniform in the cross-sectional plane and thus neglects the asymmetry in the wall temperature distribution created by the close juxtaposition of the central artery and vein. Recently, Wissler [19] has presented an exact solution for the perfect countercurrent heat exchange between paired vessels in an infinite medium which includes this asymmetry. In this solution there is a linear and equal axial temperature gradient in the medium and vessels, and the physical properties of the fluid and medium are identical and constant throughout the region.

The objective of this paper is to present a more general three-dimensional approximate analytic solution for the unequal axial countercurrent heat transfer between parallel paired vessels asymmetrically embedded in a long cylinder with surface convection, as shown in Fig. 1. Taking the reciprocal of the Peclet number as a small parameter, a perturbation method is employed to obtain the solution to the temperature distributions both in the vessels and the surrounding cylinder. The analysis introduces several important modifications of Wissler's [19] basic approach. The line heat source and sink used to replace the convective heat loss/gain from each vessel are unknown functions of the axial coordinate and are related to the local bulk fluid temperature gradients. The surrounding cylinder has a general convective boundary condition, which leads to an unknown axial variation of the heat transfer between the vessels and the vessel pair with the environment. The solution also allows for a lowest order asymmetric positioning of the vessels within the cylinder.

Results will be presented for the temperature distributions inside and outside the vessels for several representative cases. The region of biological interest

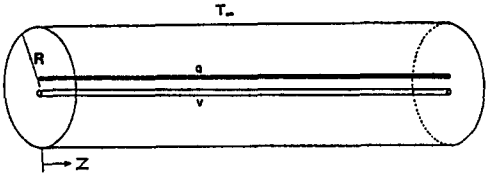

FIG. 1. Schematic of the embedding medium cylinder surrounding the countercurrent vessel pair.

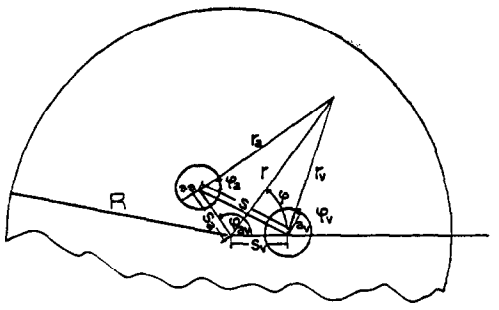

FIG. 2. Geometry of the cross-sectional plane and the coordinate system.

constitutes a small portion of these results. Explicit expressions are obtained for the vessel Nusselt number and the conduction shape factors and the results are compared with the predictions of the models by Baish *et al.* [6] and Chato [2] for uniform vessel wall temperature. An important and surprising result is that the Nusselt number is the same as for the fully developed flow in a pipe with a constant wall heat flux. The theory is then used to develop a simple prototype model for the axial temperature distributions along the central artery and vein of a human limb in which the skin temperature is unknown and allowed to vary in both the axial and angular directions. The predictions of this model are compared with results of an earlier one-dimensional model by Mitchell and Myers [12] in which the skin temperature variation is not considered. The new model is shown to provide much better agreement with the experimental data of Bazett *et al.* [20] for the axial variation of the central artery and vein temperatures.

2. FORMULATION

A steady state temperature field is assumed in both the vessels and the surrounding cylinder. The analysis further assumes that the velocity profile in the vessels is parabolic (laminar flow)† and the Peclet number is large compared to unity. The vessels are asymmetrically located at the central area of the cylinder, as shown in Fig. 2, and it is assumed that the radius of the cylinder is several times larger than the distances from the origin to the vessels. We shall also assume that the cylinder is sufficiently long for end effects to be neglected.

We introduce non-dimensional parameters and variables as follows:

$$Pe = \frac{2\rho_f c_f a_a V_a}{k_f}, \quad k' = \frac{k_f}{k_t}, \quad V' = \frac{V_a}{V_v}$$

$$\beta = \frac{1}{Pe}, \quad Bi = \frac{hR}{k_t}, \quad \bar{s} = \frac{s}{a_a}$$

$$\bar{s}_a = \frac{s_a}{a_a}, \quad \bar{s}_v = \frac{s_v}{a_a}, \quad \bar{a}_v = \frac{a_v}{a_a}, \quad \rho_R = \frac{R}{a_a}$$

$$\rho = \frac{r}{a_a}, \quad \rho_a = \frac{r_a}{a_a}, \quad \rho_v = \frac{r_v}{a_v}$$

$$z = \frac{Z}{a_a Pe}, \quad \theta = \frac{T - T_\infty}{T_0 - T_\infty}.$$

Although the theory is much more general in its application, we have used the biological notation where a and v represent an artery and vein. The governing dimensionless equations in vessel a and vessel v can be written as

$$\frac{1}{\rho}\frac{\partial}{\partial\rho}\left(\rho\frac{\partial\theta_a}{\partial\rho}\right) + \frac{1}{\rho^2}\frac{\partial^2\theta_a}{\partial\phi^2} + \beta^2\frac{\partial^2\theta_a}{\partial z^2} = (1-\rho_a^2)\frac{\partial\theta_a}{\partial z} \quad \text{for} \quad \rho_a < 1 \quad (1)$$

$$\frac{1}{\rho}\frac{\partial}{\partial\rho}\left(\rho\frac{\partial\theta_v}{\partial\rho}\right) + \frac{1}{\rho^2}\frac{\partial^2\theta_v}{\partial\phi^2} + \beta^2\frac{\partial^2\theta_v}{\partial z^2} = -V'(1-\rho_v^2)\frac{\partial\theta_v}{\partial z} \quad \text{for} \quad \rho_v < 1. \quad (2)$$

In the embedding medium, where there is no flow, the energy equation is

$$\frac{1}{\rho}\frac{\partial}{\partial\rho}\left(\rho\frac{\partial\theta_t}{\partial\rho}\right) + \frac{1}{\rho^2}\frac{\partial^2\theta_t}{\partial\phi^2} + \beta^2\frac{\partial^2\theta_t}{\partial z^2} = 0 \quad \text{for} \quad \rho_a \geqslant 1 \quad \text{and} \quad \rho_v \geqslant 1. \quad (3)$$

The dimensionless boundary conditions are

$$\theta_{a,v} = \theta_t \quad \text{at} \quad \rho_{a,v} = 1 \quad (4)$$

$$k'\frac{\partial\theta_{a,v}}{\partial\rho_{a,v}} = \frac{\partial\theta_t}{\partial\rho_{a,v}} \quad \text{at} \quad \rho_{a,v} = 1 \quad (5)$$

$$\frac{\partial\theta_t}{\partial\rho} = -\frac{Bi}{\rho_R}\theta_t \quad \text{at} \quad \rho = \rho_R. \quad (6)$$

Examination of equations and boundary conditions (1)–(6) reveals that a perturbation solution for $\theta_{a,v}$ and θ_t can be sought in the form $\theta = \theta_0 + \beta\theta_1 + O(\beta^2)$, since $\beta \ll 1$ for large Pe. Equations (1)–(3) reduce to $O(1)$ to

$$\frac{1}{\rho}\frac{\partial}{\partial\rho}\left(\rho\frac{\partial\theta_{a0}}{\partial\rho}\right) + \frac{1}{\rho^2}\frac{\partial^2\theta_{a0}}{\partial\phi^2} = (1-\rho_a^2)\frac{\partial\theta_{a0}}{\partial z} \quad \text{for} \quad \rho_a < 1 \quad (7)$$

$$\frac{1}{\rho}\frac{\partial}{\partial\rho}\left(\rho\frac{\partial\theta_{v0}}{\partial\rho}\right) + \frac{1}{\rho^2}\frac{\partial^2\theta_{v0}}{\partial\phi^2} = -V'(1-\rho_v^2)\frac{\partial\theta_{v0}}{\partial z} \quad \text{for} \quad \rho_v < 1 \quad (8)$$

$$\frac{1}{\rho}\frac{\partial}{\partial\rho}\left(\rho\frac{\partial\theta_{t0}}{\partial\rho}\right) + \frac{1}{\rho^2}\frac{\partial^2\theta_{t0}}{\partial\phi^2} = 0 \quad \text{for} \quad \rho_a \geqslant 1 \quad \text{and} \quad \rho_v \geqslant 1. \quad (9)$$

Equations (7) and (8) are complicated by the con-

† The Reynolds number in the arm or leg is typically 1000 or less for humans.

vective terms on their right-hand side. The partial derivatives $\partial\theta_{a0}/\partial z$ and $\partial\theta_{v0}/\partial z$ are required to describe the entrance and exit regions at the cylinder ends where the temperature profiles develop from their initial conditions. Away from these end regions we assume the local temperature profiles can be related to the local axial temperature gradients in the fluid in much the same way that a velocity profile can be described by its streamwise pressure gradient. The choice of which temperature gradient to use (centerline, average, bulk, etc.) is subtle and will be discussed later. Thus, the temperature gradients in the convection terms on the right-hand side of equations (7) and (8) can be approximated by $d\theta_{ac}/dz$ and $d\theta_{vc}/dz$ in vessels a and v, respectively, where $d\theta_{ac}/dz$ and $d\theta_{vc}/dz$ are unknown characteristic axial gradients in each vessel. This approximation greatly simplifies the equations since the infinite series of eigenvalues required to describe the axial development of the temperature profiles for the full equations (7) and (8) will be reduced to two characteristic eigenvalues describing the axial interaction of θ_{ac} and θ_{vc}.

3. SOLUTION PROCEDURE

The solution for θ_{a0}, θ_{v0}, θ_{t0}, which we denote by θ_0, can be decomposed into two parts

$$\theta_0 = \theta_H + \theta_P \tag{10}$$

where θ_H is a homogeneous solution, and θ_P a particular solution. θ_P is defined as

$$\theta_P = -Q_a\theta_{pa} + Q_v\theta_{pv} \tag{11}$$

in which

$$Q_a = -\frac{1}{4}\frac{d\theta_{ac}}{dz} \tag{12}$$

$$Q_v = -\tfrac{1}{4}V'\bar{a}_v^2\frac{d\theta_{vc}}{dz} \tag{13}$$

$$\theta_{Pa,v} = \begin{cases}\rho_{a,v}^2 - \frac{1}{4}\rho_{a,v}^4 - \frac{3}{4} \\ k'\ln\rho_{a,v}\end{cases} \quad \text{for} \quad \begin{cases}\rho_{a,v} < 1 \\ \rho_{a,v} \geqslant 1\end{cases}. \tag{14}$$

It is easily shown that θ_P satisfies equations (4) and (7)–(9) with the replacement of total for partial derivatives on the right-hand side of equations (7) and (8), but cannot satisfy equation (5) exactly unless $k' = 1$. However, the vessels are much smaller than the cylinder so that θ_P is a reasonable approximate solution when $k' \approx 1$. To satisfy boundary condition (6), we first expand θ_P as a power series in $\bar{s}_{a,v}/\rho$ and neglect terms of $O(\bar{s}_{a,v}^2/\rho_R^2)$. We now require that $\theta_H + \theta_P$ satisfy equation (6) at $\rho = \rho_R$. One obtains the approximate homogeneous solution after the unknown coefficients are evaluated

$$\theta_H = k'\left[\left(\frac{1}{Bi} + \ln\rho_R + \frac{(Bi-1)\bar{s}_a}{(1+Bi)\rho_R^2}\rho\cos(\phi-\phi_{av})\right)\right]Q_a - k'\left[\left(\frac{1}{Bi} + \ln\frac{\rho_R}{\bar{a}_v} - \frac{(Bi-1)\bar{s}_v}{(1+Bi)\rho_R^2}\rho\cos\phi\right)\right]Q_v. \tag{15}$$

Hence, equation (10) can be written in the form

$$\theta_0 = \frac{1}{4}\left[\left(-\frac{1}{Bi} - \ln\rho_R - \frac{(Bi-1)\bar{s}_a}{(1+Bi)\rho_R^2}\rho\cos(\phi-\phi_{av})\right)k' + \theta_{pa}\right]\frac{d\theta_a}{dz} + \tfrac{1}{4}\bar{a}_v^2V'\left[\left(\frac{1}{Bi} + \ln\frac{\rho_R}{\bar{a}_v} - \frac{(Bi-1)\bar{s}_v}{(1+Bi)\rho_R^2}\rho\cos\phi\right)k' - \theta_{pv}\right]\frac{d\theta_v}{dz} \tag{16}$$

where θ_{pa} and θ_{pv} differ according to the regions defined in equation (14). Equation (16) describes the ϕ dependence both in the vessels and the surrounding cylinder.

If the solution (16) is substituted in equations (7) and (8) and the equations are integrated over the cross-sectional area of each vessel, one finds that the resulting integrated average equation will be satisfied only if θ_{ac} and θ_{vc} are the zeroth-order bulk temperatures θ_{ab0} and θ_{vb0}. The characteristic axial gradients $d\theta_{ac}/dz$ and $d\theta_{vc}/dz$ therefore are replaced by their corresponding bulk temperature gradients $d\theta_{ab0}/dz$ and $d\theta_{vb0}/dz$.

Substituting solution (16) for θ_a and θ_v into the definitions of the bulk temperatures

$$\theta_{a,vb} = \frac{2}{\pi}\int_0^{2\pi}\int_0^1 \theta_{a,v}(1-\rho_{a,v}^2)\rho_{a,v}\,d\rho_{a,v}\,d\phi_{a,v} \tag{17}$$

and evaluating these double integrals, one obtains the differential equations for θ_{ab0} and θ_{vb0}

$$\theta_{ab0} = \frac{1}{4}\left[\left(-\frac{1}{Bi} - \ln\rho_R\right)k' - \frac{11}{24}\right]\frac{d\theta_{ab0}}{dz} + \tfrac{1}{4}\bar{a}_v^2V'k'\left(\frac{1}{Bi} + \ln\frac{\rho_R}{\bar{s}\bar{a}_v}\right)\frac{d\theta_{vb0}}{dz} \tag{18}$$

$$\theta_{vb0} = \frac{k'}{4}\left(-\frac{1}{Bi} - \ln\frac{\rho_R}{\bar{s}}\right)\frac{d\theta_{ab0}}{dz} + \tfrac{1}{4}\bar{a}_v^2V'\left[\left(\frac{1}{Bi} + \ln\frac{\rho_R}{\bar{a}_v}\right)k' + \frac{11}{24}\right]\frac{d\theta_{vb0}}{dz}. \tag{19}$$

The coupled linear equations (18) and (19) have solutions of the form

$$\theta_{ab0} = C_1A_{11}\exp(\lambda_1 z) + C_2A_{21}\exp(\lambda_2 z) \tag{20}$$

$$\theta_{vb0} = C_1A_{12}\exp(\lambda_1 z) + C_2A_{22}\exp(\lambda_2 z) \tag{21}$$

where eigenvalues λ_i are given by

$$\lambda_{1,2} = \frac{-b \pm \sqrt{(b^2 - 16a)}}{a} \tag{22}$$

with

$$a = \bar{a}_v^2V'\left[\left(\frac{1}{Bi} + \ln\frac{\rho_R}{\bar{a}_v}\right)k' + \frac{11}{24}\right]\left[\left(-\frac{1}{Bi} - \ln\rho_R\right)k' - \frac{11}{24}\right] - \bar{a}_v^2V'^2k'^2\left(\frac{1}{Bi} + \ln\frac{\rho_R}{\bar{s}\bar{a}_v}\right)\left(-\frac{1}{Bi} - \ln\frac{\rho_R}{\bar{s}}\right)$$

$$b = 2\left(\frac{1}{Bi}+\ln\rho_R+\frac{11}{24}\right)-2\bar{a}_v^2V'\left[\left(\frac{1}{Bi}+\ln\frac{\rho_R}{\bar{a}_v}\right)k'+\frac{11}{24}\right]$$

A_{ij} are the eigenvector coefficients of the equations and C_1 and C_2 are constants which are determined by the prescribed bulk temperatures at any station of the vessels.

4. RESULTS

Since the temperatures within the vessels are non-uniform and the mean temperature of the surrounding cylinder in the cross-sectional plane varies along the axial direction, it is appropriate to compute the mean temperature of the cylinder and to define the heat conduction shape factors in terms of the differences in the bulk temperatures, and mean medium and environmental temperatures. Because the area of the vessels is small compared to the area of the cylinder in the cross-sectional plane, the mean temperature of the cylinder at each cross-section can be approximated by

$$\theta_{tm0} \approx \frac{1}{\pi\rho_R^2}\int_0^{\rho_R}\int_0^{2\pi}\theta_0\rho\,d\phi\,d\rho = -\frac{k'}{4}\left(\frac{1}{Bi}+\frac{1}{2}\right)\left(\frac{d\theta_{ab0}}{dz}-\bar{a}_v^2V'\frac{d\theta_{vb0}}{dz}\right). \quad (23)$$

The mean excess wall temperatures of the vessels can also be computed as follows:

$$\theta_{aw0} = \frac{1}{2\pi}\int_0^{2\pi}\theta_{a0}\,d\phi_a = \frac{k'}{4}\left(-\frac{1}{Bi}-\ln\rho_R\right)\frac{d\theta_{ab0}}{dz} + \tfrac{1}{4}\bar{a}_v^2V'k'\left[\frac{1}{Bi}+\ln\frac{\rho_R}{\bar{s}\bar{a}_v}\right]\frac{d\theta_{vb0}}{dz} \quad (24)$$

$$\theta_{vw0} = \frac{1}{2\pi\bar{a}_v}\int_0^{2\pi}\theta_{v0}\,d\phi_v = \frac{k'}{4}\left(-\frac{1}{Bi}-\ln\frac{\rho_R}{\bar{s}}\right)\frac{d\theta_{ab0}}{dz} + \tfrac{1}{4}\bar{a}_v^2V'k'\left[\frac{1}{Bi}+\ln\frac{\rho_R}{\bar{a}_v}\right]\frac{d\theta_{vb0}}{dz}. \quad (25)$$

The Nusselt number of vessel a is defined as

$$Nu_{a0} = \frac{q_{a0}}{\pi k_f(T_{ab0}-T_{aw0})} = -\frac{\pi\rho_f c_f a_a^2\dfrac{dT_{ab0}}{dz}}{\pi k_f(T_{ab0}-T_{aw0})} = \frac{48}{11}. \quad (26)$$

It is easily shown that the Nusselt number of vessel v, Nu_{v0}, has this same value. This value is also the same as for the fully developed temperature profile in a single pipe with a constant heat flux to the environment. For the present solution, the net integrated heat flux from each vessel at any station is determined only by the particular solution in equation (14). This solution is locally the same as the solution for fully developed flow in a pipe with a constant axial temperature gradient. The homogeneous solution (15) does not contribute to the net heat flux since it does not contain heat sources or sinks.

Results (23)–(26) can be used to obtain the expressions for the conduction shape factors σ_{c0} and σ_{t0} describing the heat transfer between the vessels, and between the vessel pair and the environment. These expressions are

$$\sigma_{c0} = \frac{q_{a0}-q_{v0}}{\pi k_t(T_{ab0}-T_{vb0})} = \frac{2}{\dfrac{11}{24}+k'\ln\bar{s}} \quad (27)$$

$$\sigma_{t0} = \frac{q_{a0}+q_{v0}}{\pi k_t(T_{tm0}-T_\infty)} = \frac{4Bi}{k'(2+Bi)}. \quad (28)$$

It is interesting to note that to $O(\bar{s}_{a,v}^2/\rho_R^2)$, σ_{c0} depends on the spacing of the vessels only rather than their asymmetry with respect to the origin, and σ_{t0} is a simple function of the cylinder Biot number.

For convenience, we let the polar angle $\phi_{av} = \pi$ and $s_s = s_v$ in all the following calculations. The bulk fluid and mean embedding medium temperature distribution $\theta_{a,vb0}$ and θ_{tm0} along the axial coordinate for $Bi = 0.5$ and 10, which are typical values for the human upper limb in air and water respectively, are shown in Figs. 3 and 4. The solution exhibits a saddle point behavior. For each case, there is a critical temperature of vessel v at $Z = 0$, $\bar{\theta}_{vb}(0)$, which separates two families of solutions. This critical temperature corresponds to a very long cylinder with the right end

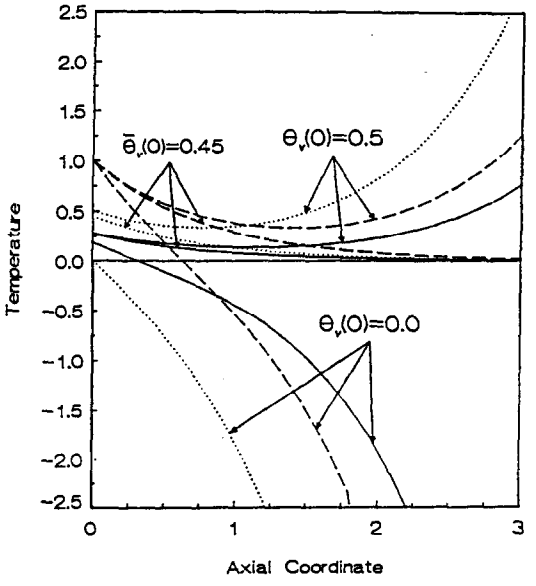

FIG. 3. Bulk temperature distributions in the vessels and axial profile of the mean embedding medium temperature at the cross-sectional plane for three different axial boundary conditions $\theta_{vb}(0)$. $Bi = 0.5$, $k' = 1$, $\bar{s} = 2.1$, $\rho_R = 10$, $\bar{a}_v = 1$. ---, a; ···, v; ——, mean.

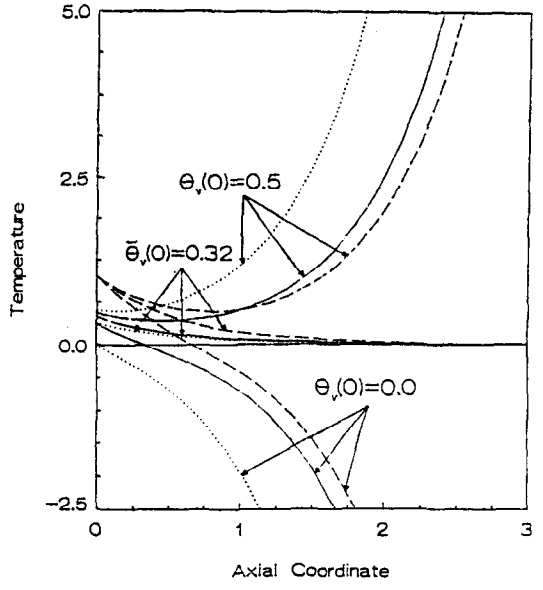

FIG. 4. Bulk temperature distributions in the vessels and axial profile of the mean embedding medium temperature at the cross-sectional plane for three different axial boundary conditions $\theta_{vb}(0)$. $Bi = 10$, $k' = 1$, $\bar{s} = 2.1$, $\rho_R = 10$, $\bar{a}_v = 1$. ---, a; ···, v; ——, mean.

maintained at the ambient temperature. As the Biot number is increased from 0.5 to 10, $\bar{\theta}_{vb}(0)$ decreases from 0.45 to 0.32. The dimensionless bulk temperatures grow exponentially positive or negative depending upon whether the bulk temperature $\theta_{vb}(0)$ is greater or less than the critical value. In addition, the mean embedding medium temperature need not lie between the bulk temperatures of the vessels, as we assumed in ref. [10] for the case of small heat loss from a tissue cylinder in the microcirculation. Figures 5 and 6 show the non-uniform circumferential temperature distribution at the vessel walls and the cylinder surface at three different axial cross-sections for $\theta_{vb}(0) = 0.5$, and $Bi = 0.5$ and 10, respectively.

5. DISCUSSION

5.1. *General behavior*

To evaluate the validity of the assumption that the axial temperature gradients in the convection terms of equations (1) and (2) can be approximated by the bulk temperature gradients, the normalized difference between the local and bulk axial temperature gradients

$$\left(\frac{\partial\theta_{a,v}}{\partial z} - \frac{d\theta_{a,vb}}{dz}\right)\Big/\frac{d\theta_{a,vb}}{dz}$$

has been calculated. Figure 7 shows the difference distribution across vessel a for the axial boundary condition $\theta_{vb}(0) = 0.9$ and 0.5 at $z = 0$. The maximum value of this normalized difference in the cross-sectional plane occurs at the point in closest proximity to the other vessel. The maximum deviation is less than 19% for the boundary value problems in Figs. 3, 4 and 8. Thus, it is reasonable to approximate the axial temperature gradients in equations (7) and (8) by their bulk temperature gradients.

It is interesting to note that the temperature profiles in the vessels do not satisfy the definition of a fully developed temperature profile

$$\frac{\partial}{\partial z}\left(\frac{\theta_{a,v} - \theta_{a,vw}}{\theta_{a,vb} - \theta_{a,vw}}\right) = 0 \qquad (29)$$

throughout the vessels even though the Nusselt numbers of the vessels remain constant. The temperature profiles in the vessels continue to deviate somewhat from a fully developed profile due to the countercurrent axial interaction, regardless of the axial distance from the entrance. However, the fully developed temperature profile defined in equation (29) is satisfied only for a constant axial temperature gradient in the vessels and surrounding medium as shown in ref. [19]. The temperature profile (16) can thus be viewed as a quasi fully developed profile in which the Nusselt number does not change but the bulk temperature gradients slowly change to account for the heat loss at the cylinder surface and the axial interaction between the vessels.

Since the present analysis assumes that the vessels are located in the central area of the cylinder and neglects terms of $O(\bar{s}_{a,v}^2/\rho_R^2)$, the heat transfer between vessels and cylinder is determined by the relative spacing of the vessels and not the asymmetry with respect to the cylinder. In other words, to $O(\bar{s}_{a,v}^2/\rho_R^2)$ the heat transfer will not change when the vessels are displaced as a pair from the origin. This partly explains why the bulk and mean wall temperatures of the vessels are independent of the asymmetry parameters $\bar{s}_a$ and $\bar{s}_v$ but depend on the distance between the vessels and the ratio of their radii.

From Figs. 3 and 4, one observes that when $\theta_{vb}(0) = 0.5$, the bulk temperatures θ_{ab0} and θ_{vb0} have a crossover point. The axial position of this point decreases and the temperature distribution changes more significantly along the axial coordinate when the Biot number is increased from 0.5 to 10. Depending on the Biot number and the bulk temperature $\theta_{vb}(0)$, the mean embedding medium temperature θ_{tm0} relative to that of vessel a may change along the cylinder. For $Bi = 0.5$ and $\theta_{vb}(0) = 0$, θ_{tm0} shifts from a level below the bulk temperature of vessel a to one above at $z \approx 0.9$ as shown in Fig. 3. However, no such crossover is observed for this case when the Biot number is increased to 10 (Fig. 4). A similar behavior is obtained for $\theta_{vb}(0) = 0.5$. Thus the direction of heat flow between the vessels and between the embedding medium and vessels may change along the cylinder, depending on $\theta_{vb}(0)$ and the Biot number of the cylinder which describes the heat loss to the environment.

In Table 1 results for σ_{c0} for several representative blood vessel pairs are compared with the predictions of Baish *et al.* [6] and Chato [2]. In ref. [2] the vessels

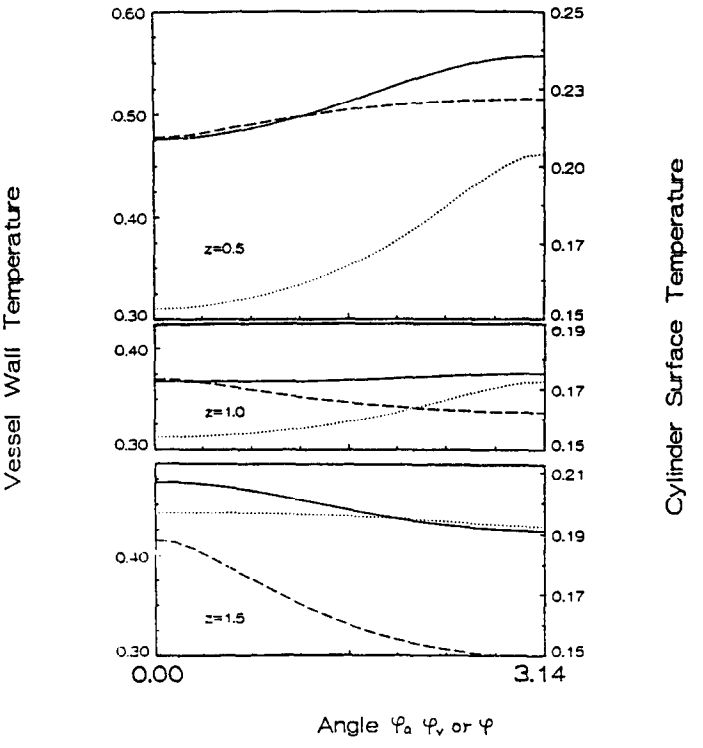

FIG. 5. Angular temperature distributions at the vessel walls and the cylinder surface under the same conditions as Fig. 3 at three different cross-sections for $s_a = s_v$, $\phi_{av} = \pi$ and $\theta_{vb}(0) = 0.5$. ---, a; ···, v; ——, surface.

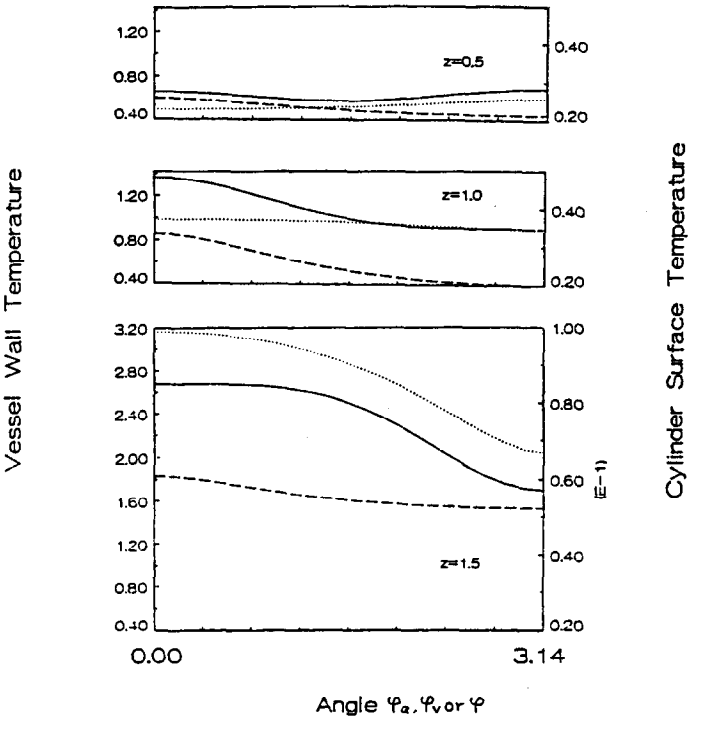

FIG. 6. Angular temperature distributions at the vessel walls and the cylinder surface under the same conditions of Fig. 4 at three different cross-sections for $s_a = s_v$, $\phi_{av} = \pi$ and $\theta_{vb}(0) = 0.5$. ---, a; ···, v; ——, surface.

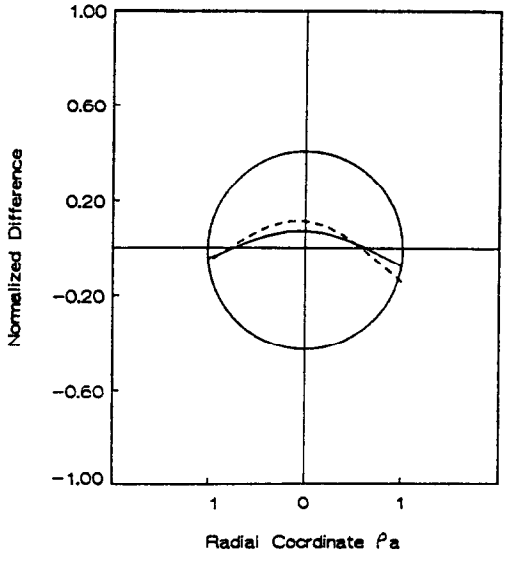

FIG. 7. Variation of the normalized difference between the local and bulk axial temperature gradients in the cross-sectional plane $z = 0$. $Bi = 0.5$, $k' = 1$, $\bar{s} = 2.1$, $\rho_R = 10$, $\bar{a}_v = 1$. ——, $\theta_{vb}(0) = 0.9$; - - -, $\theta_{vb}(0) = 0.5$.

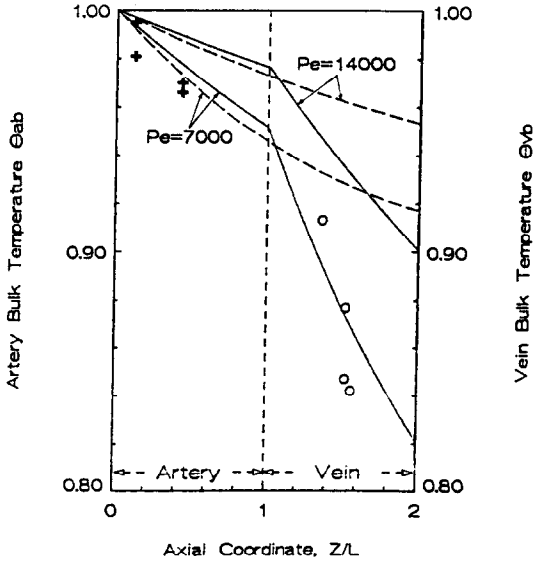

FIG. 8. Comparison of the bulk temperature distributions in the central vessels of a limb predicted by the present model and the Mitchell and Myers' model [12] with the experimental data for Bazett *et al.* [20]. $Bi = 1.5$, $k' = 1$, $\bar{s} = 4$, $\bar{a}_v = 1$, $\rho_R = 16$. ——, present; - - -, ref. [12]; +, ○, ref. [20].

are embedded in an infinite medium whereas in ref. [6] the surrounding cylinder has a uniform surface temperature. In the present solution σ_{c0} is based on the difference between the bulk vessel temperatures, while in refs. [2, 6] it is based on the difference between the vessels, surface temperatures which are assumed uniform. This partly explains why the present model gives lower values for σ_{c0}. As the spacing between vessels is decreased from 2.5 to 2.1, the effect of surface temperature nonuniformity on σ_{c0} becomes more important, resulting in much lower values for σ_{c0} than predicted by the uniform wall temperature models [2, 6]. The solutions in Figs. 5 and 6 clearly show the large variation in wall temperature.

5.2. *Application to whole limb heat transfer*

In Fig. 8 the experimental data of Bazett *et al.* [20] for the axial temperature distribution for the artery and vein in a limb is compared with the present model and that of Mitchell and Myers [12]. Both models assume (a) constant blood flow rates in the vessels, (b) metabolic and perfusion heat sources in the surrounding tissue cylinder are negligible, (c) all blood and tissue properties are constant, (d) the temperatures of the artery and vein are equal at the wirst end. An important difference between the two models is that the variation of the skin surface temperature is neglected in ref. [12]. Thus in ref. [12] constant overall heat transfer coefficients are assumed to characterize the heat transfer between vessels, and between vessels and the environment for a one-dimensional countercurrent exchange. Using the same geometrical parameters, the present theory is applied to determine the artery and vein axial temperature distribution for $Bi = 1.5$, which accounts for the radiation heat transfer, and two Peclet numbers 7000 and 14 000, which are typical of the arm at rest and during light exercise. For the limb the dimensionless coordinate z is typically confined to the region $z < 0.07$. Figure 8, therefore, corresponds only to a small portion of Figs. 3 and 4. It is clear that the present model provides a much better agreement with experimental data for the axial artery and vein temperature distribution than the Mitchell and Myers' model.

The whole limb model developed in ref. [13] is much more elaborate than the simple axial interaction models just discussed. This more detailed model considers the local arterial bleed off and venous return

Table 1. Shape factor σ_c for equal sized vessels

Type of vessel	a_a (μm)	ρ_R	$\bar{s}$	σ_c Present	σ_c Ref. [6]	σ_c Ref. [2]
Large artery	1500	40	2.5	1.455	1.679	1.682
Medium artery	500	35	2.5	1.455	1.677	1.682
Small artery	200	20	2.1	1.666	3.159	3.175

from the central vessels to the muscle tissue and the cutaneous circulation, the variation of the effective tissue conductivity due to blood perfusion as a function of depth from the skin surface and the local variation in diameter of the arm and the central supply vessels as one proceeds from the shoulder toward the wrist. This model predicts a radial temperature profile which agrees well with the experimental data in ref. [21] but inadequately describes the axial temperature variation when the heat loss from the limb is large. In general, the results of Song *et al.* [13] and Mitchell and Myers [12] indicate that the heat loss to the environment is comparable or larger than the heat exchange between the central vessels. This failing of the model in ref. [13] stems from an approximation introduced in deriving the expression for the central artery–vein temperature difference and the average core temperature which assumes that the heat loss to the surroundings is small compared to the heat exchange between the central vessels. The present model, which is not limited by this restriction, can be readily incorporated within the general formulation outlined in ref. [13] in one of several ways that are currently being explored. Equations (1) and (2) could be modified to allow for the z variation of the flow in the central artery and vein due to the bleed off, equation (3) solved with an effective conductivity in the radial direction that is determined by the Weinbaum–Jiji equation and the z variation of ρ_R included in boundary condition (6). Alternatively, the limb could be divided into a small number of axial segments in which the vascular geometry and flow and tissue properties are assumed to be independent of the z variable in each segment, but at the interface between segments there is a discontinuity in the flow and geometry to account for the local bleed off from the central supply vessels and the tapering of the limb.

Acknowledgement—This research was supported by NSF Grant GBT-8702582 and was performed in partial fulfillment of the requirements for the Ph.D. degree of Min Zhu from the City University of New York.

REFERENCES

1. W. M. Kays and A. C. London, *Compact Heat Exchangers*. McGraw-Hill, New York (1986).
2. J. C. Chato, Heat transfer to blood vessels, *ASME J. Biomech. Engng* **102**, 110–118 (1980).
3. S. Weinbaum, L. M. Jiji and D. E. Lemons, Theory and experiment for the effect of blood vascular microstructure on surface tissue heat transfer. Part I: anatomical foundation and model conceptualization, *ASME J. Biomech. Engng* **106**, 321–330 (1984).
4. L. M. Jiji, S. Weinbaum and D. E. Lemons, Theory and experiment for the effect of blood vascular microstructure on surface tissue heat transfer. Part II: model formulation and solution, *ASME J. Biomech. Engng* **106**, 331–341 (1984).
5. S. Weinbaum and L. M. Jiji, A new simplified bioheat equation for the effect of blood flow on local average tissue temperature, *ASME J. Biomech. Engng* **107**, 131–139 (1985).
6. J. W. Baish, P. S. Ayyaswamy and K. R. Foster, Small-scale temperature fluctuations in perfused tissue during local hyperthermia, *ASME J. Biomech. Engng* **108**, 246–250 (1986).
7. J. W. Baish, P. S. Ayyaswamy and K. R. Foster, Heat transport mechanism in vascular tissues: a model comparison, *ASME J. Biomech. Engng* **108**, 324–331 (1986).
8. D. E. Lemons, S. Weinbaum and L. M. Jiji, Experimental studies on the role of micro and macro vascular system in tissue heat transfer, *Am. J. Physiol.* **253**, R128–R135 (1987).
9. E. H. Wissler, Comments on the new bioheat equation proposed by Weinbaum and Jiji, *ASME J. Biomech. Engng* **109**, 226–233 (1987).
10. M. Zhu, S. Weinbaum, L. M. Jiji and D. E. Lemons, On the generalization of the Weinbaum–Jiji bioheat equation to microvessels of unequal size; the relation between the near field and local average tissue temperatures, *ASME J. Biomech. Engng* **110**, 74–81 (1988).
11. C. K. Charny and R. L. Levin, Heat transfer normal to paired arteries and veins embedded in perfused tissue during hyperthermia, *ASME J. Biomech. Engng* **110**, 277–282 (1988).
12. J. W. Mitchell and G. E. Myers, An analytical model of the countercurrent heat exchange phenomenon, *Biophys. J.* **8**, 897–911 (1968).
13. W. J. Song, S. Weinbaum, L. M. Jiji and D. E. Lemons, A combined macro and microvascular model for whole limb heat transfer, *ASME J. Biomech. Engng* **110**, 259–268 (1988).
14. E. R. G. Eckert and R. M. Drake, *Analysis of Heat and Mass Transfer*, pp. 98 and 340. McGraw-Hill, New York (1972).
15. E. Hahne and U. Grigull, A shape factor scheme for point source configurations, *Int. J. Heat Mass Transfer* **17**, 267–273 (1974).
16. R. Thiyagarajan and M. M. Yovanovich, Thermal resistance of a buried cylinder with constant flux boundary condition, *ASME J. Heat Transfer* **96**, 249–250 (1974).
17. R. F. DiFelice, Jr. and H. H. Bau, Conductive heat transfer between eccentric cylinders with boundary conditions of the third kind, *ASME J. Heat Transfer* **105**, 678–680 (1983).
18. H. H. Bau and S. S. Sadhal, Heat losses from a fluid flowing in a buried pipe, *Int. J. Heat Mass Transfer* **25**, 1621–1629 (1982).
19. E. H. Wissler, An analytical solution for countercurrent heat transfer between parallel vessels with a linear axial temperature gradient, *ASME J. Biomech. Engng* **110**, 254–256 (1988).
20. H. C. Bazett, L. Love, M. Newton, L. Eisenberg, R. Day and R. Forster II, Temperature changes in blood flowing in arteries and veins in man, *J. Appl. Physiol.* **1**, 3–19 (1948).
21. H. H. Pennes, Analysis of tissue and arterial blood temperature in the resting forearm, *J. Appl. Physiol.* **1**, 93–122 (1948).

ECHANGE THERMIQUE ENTRE DES RECIPIENTS NOYES DE FACON DISSYMETRIQUE DANS UN CYLINDRE AVEC CONVECTION A LA SURFACE

Résumé— Une solution analytique approchée tridimentionnelle est présentée pour le transfert thermique à contre-courant entre deux récipients parallèles noyés de façon dissymétrique dans un cylindre long avec convection à la surface. L'analyse suppose que le profil de vitesse dans les récipients est parabolique, que le nombre de Peclet est grand par rapport à l'unité et que le rayon du cylindre est plusieurs fois plus grand que les distances du centre du cylindre aux récipients. Une méthode de perturbation est utilisée en prenant l'inverse du nombre de Peclet comme paramètre petit. La nouvelle approche prend en considération l'interaction thermique axiale et décrit le champ thermique dissymétrique tridimensionnel dû aux températures pariétales non uniformes des récipients dans le plan transversal. On discute l'application du modèle à l'ensemble.

WÄRMEÜBERTRAGUNG ZWISCHEN UNGLEICHEN, IM GEGENSTROM ANGEORDNETEN BEHÄLTERN, DIE UNSYMMETRISCH IN EINEM ZYLINDER MIT KONVEKTION AN DER OBERFLÄCHE EINGEBAUT SIND

Zusammenfassung—Für den Wärmeübergang im Gegenstrom zwischen parallel angeordneten Behältern wird eine dreidimensionale Näherungslösung vorgestellt. Die Behälter befinden sich in einem langen Zylinder, an dessen Oberfläche Konvektion auftritt, und sind asymmetrisch angeordnet. Bei der Untersuchung wird angenommen, daß das Strömungsprofil in den Behältern parabolisch, die Peclet-Zahl deutlich größer als 1 ist und daß der Radius des Zylinders ein Mehrfaches des Abstandes zwischen Zylinderachse und Behältern beträgt. Ein Störungsverfahren wird verwendet, indem der Kehrwert der Peclet-Zahl als kleiner Wert angenommen wird. Das neue Verfahren berücksichtigt die thermischen Vorgänge in axialer Richtung und beschreibt das dreidimensionale asymmetrische Temperaturfeld, das sich aufgrund der in Querschnittsebene nicht einheitlichen Temperatur der Behälter einstellt. Die Anwendung des Modells auf den Wärmeübergang am gesamten Schenkel wird diskutiert.

ТЕПЛООБМЕН МЕЖДУ НЕОДИНАКОВЫМИ ПРОТИВОТОЧНЫМИ ЕМКОСТЯМИ, АСИММЕТРИЧНО РАСПОЛОЖЕННЫМИ В ЦИЛИНДРЕ С КОНВЕКЦИЕЙ НА ПОВЕРХНОСТИ

Аннотация—Приводится трехмерной приближенное аналитическое решение для неодинакового противоточного теплопереноса между параллельными емкостями, расположенными попарно и асимметрично в цилиндре большой длины с конвективной теплоотдачей на поверхности. Предполагается, что профиль скоростей в сосудах является параболическим, значение числа Пекле превышает единицу, а радиус цилиндра в несколько раз больше расстояния между центром цилиндра и емкостями. Используется метод возмущений, в котором обратная величина числа Пекле считается малым параметром. Новое приближенное решекие учитывает аксиальное тепловое взаимодействие и описывает трехмерное асимметричное тепловое поле, обусловленное неоднородностью температур стенок в плоскости поперечного сечения емкостей. Обсуждается применение модели для теплопереноса во всей конструкции.